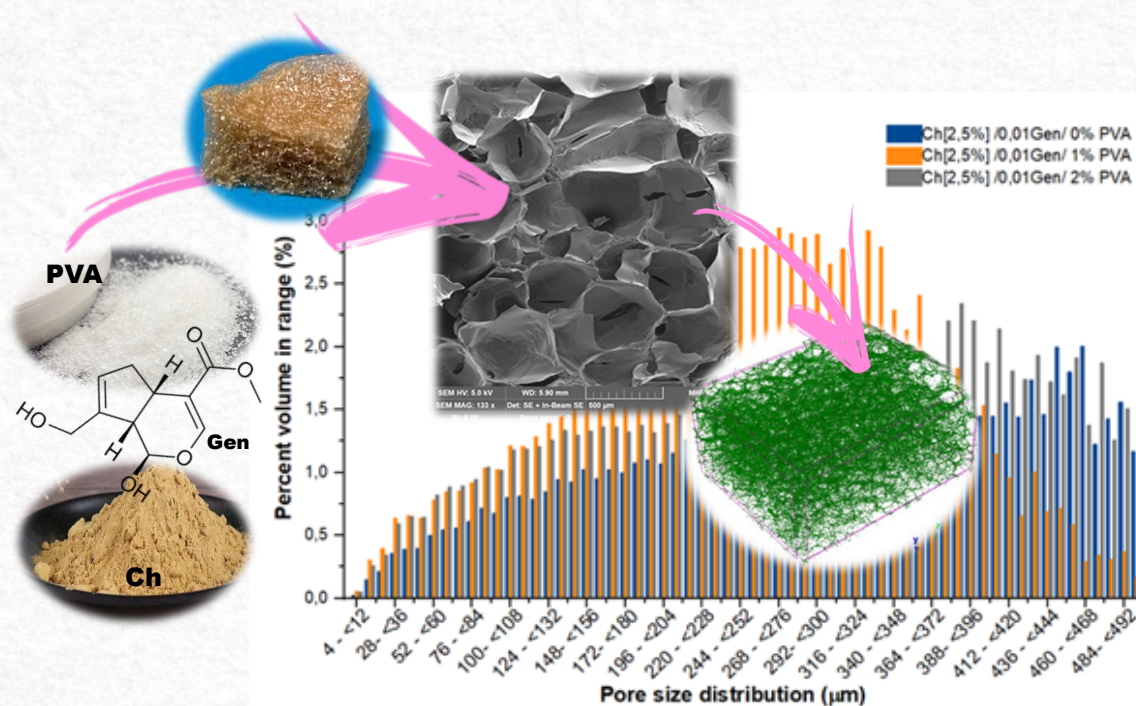


# Morphological analysis reveals the influence of genipin and polyvinyl alcohol on porous morphology on interpenetrated chitosan xerogels

M.V. Guimarães<sup>1</sup>; G.H. de Magalhães Gomes<sup>1,2</sup>; K.F. Santos<sup>1</sup>;  
J.L. Dávila<sup>1,3</sup>; L.A. Perdígón<sup>3</sup>; P.Y. Noritomi<sup>1</sup>; M.A. Sabino<sup>1,3\*\*</sup>

Received: October 2024; Accepted: December 2024.

\*Corresponding author: E-mail address: \*mvguimaraes@cti.gov.br; \*\*msabino@usb.ve



**Abstract:** The morphological characterization of xerogels composed of chitosan, genipin, and PVA demonstrates that their porous architecture is essential to their function as scaffolds for tissue engineering, with significant impacts on absorption properties, cell viability, and potential for biomedical application. SEM and microCT analysis confirmed that these xerogels possess a highly porous internal morphology, with interconnected pores forming an interpenetrating polymeric network, free from phase separation between chitosan and PVA. Hemocompatibility assays suggested the non-cytotoxic nature of these materials. Varying genipin concentrations showed that lower concentrations produce more heterogeneous pore sizes, while higher concentrations yield a uniform pore distribution, likely due to the increased availability of crosslinking sites. Additionally, the degree of anisotropy increases with both higher genipin and PVA concentrations, suggesting enhanced alignment within the three-dimensional structure. The total open pore volume, which ranges from 88% to 93%, is modifiable based on the concentrations of genipin and PVA. These insights indicate that these xerogels are viable candidates for clinical applications, particularly as potential substitutes for nucleus pulposus, given their high swelling capacity, porosity, interconnectivity, biocompatibility, and adaptable morphological characteristics.

**Keywords:** Chitosan. Genipin. Polyvinyl alcohol. SEM. MicroCT. Xerogels.

<sup>1</sup>Division DITPS, Renato Archer Center for Information Technology, Campinas, SP, Brazil.

<sup>2</sup>Federal University of Itajubá, Instituto de Ciências Puras e Aplicadas, Itabira, MG, Brazil.

<sup>3</sup>Universidad Simón Bolívar, Grupo B5IDA, Dpto. Química, Caracas, Venezuela.

## Introduction

Tissue engineering has become a key area of biomedical science, focusing on the repair and regeneration of damaged or diseased tissue. Among the numerous strategies explored, the development of three-dimensional (3D) biopolymer-based scaffolds has shown promise in replicating the architecture of the native extracellular matrix (ECM)<sup>[1]</sup>.

Chitosan, a chitin-derived biopolymer, has attracted the interest of researchers due to its biocompatibility, biodegradability and versatility in forming gels that can be used as scaffolds for cell culture<sup>[2]</sup>. For this reason, this biopolymer can help in the development of various hydrogel formulations with morphological and biomechanical properties that mimic, for example, the morphology of the intervertebral nucleus pulposus<sup>[3]</sup>. The nucleus pulposus is an essential component of the intervertebral disc and plays a fundamental role in the biomechanics and functionality of the spine. Its degeneration can lead to painful and debilitating conditions, making it a subject of great interest in traumatology<sup>[4]</sup> and the treatment of occupational diseases<sup>[5]</sup>. This emphasizes the need to establish effective strategies for its recovery.

Through the use of advanced techniques such as scanning electron microscopy (SEM) and X-ray microtomography (microCT), it is possible to analyze interpenetrating hydrogels and observe how the dispersed phase influences the porous morphology of gels<sup>[6,7]</sup> based on a biopolymer matrix such as chitosan<sup>[8]</sup>. Interpenetrating gels produced by the mechanical mixing of chitosan with polyvinyl alcohol (PVA) at different concentrations could represent an important advance in the development of scaffolds. They enable new approaches by incorporating dispersed phases, such as PVA, to create new types of interpenetrating gels. An interpenetrating gel consists of two or more polymer networks (of the same or different nature) that chemically or physically interlace but are immiscible<sup>[9]</sup>. PVA is a synthetic polymer known for its excellent rheological behavior, hydrophilicity, cell compatibility and ability to improve the mechanical and structural properties of polymer gels<sup>[10]</sup>. It is also used in the formulation of ceramic pastes for bioprinting applications<sup>[11]</sup>.

Some gels need to be crosslinked to achieve the desired behavior. In the context of chitosan, genipin, emerges as one of the most promising agents for crosslinking a natural and non-cytotoxic compound. Being a natural product, it is of great interest for some applications where its solubility in water or in ethanolic solutions at low concentration allows its easy manipulation to be incorporated into biopolymer gels; also providing enhanced structural stability to gels while maintaining their biocompatibility

<sup>[12]</sup>. Simple tests, such as hemocompatibility tests, show that the new biomaterial formulations can be safely used in biomedical applications. In addition, international technical standards (ISO and ASTM) define the test protocols for performing this type of evaluation<sup>[13-15]</sup>.

The rheological, physicochemical, mechanical and bioactive properties of these formulated gels depend directly on their internal morphology. Specialized techniques like scanning electron microscopy (SEM) and microtomography (microCT) are combined to thoroughly analyze the three-dimensional structure of the gel in its dehydrated form, or xerogel.

Scanning electron microscopy (SEM) enables the visualization of surface and internal structures at the microscale and nanoscale<sup>[16]</sup>. Microtomography (microCT) uses X-rays to produce 3D images, enabling detailed analysis of pore distribution in materials<sup>[17]</sup>. MicroCT provides additional information that cannot be obtained with SEM alone. This combined approach offers a clearer understanding of the morphological properties of the gel and establishes a foundation for future research into applications like tissue regeneration and other biotechnological uses. This is crucial because a well-developed porous structure facilitates nutrient exchange, oxygenation and cell growth within the scaffold<sup>[18]</sup>. The interconnection between pores also plays a fundamental role in facilitating adequate blood flow, which is essential for the successful integration of the implant with the surrounding tissue<sup>[19]</sup>.

This study emphasizes the benefits of using chitosan for scaffolds in tissue engineering and highlights how genipin enhances its formulation by promoting cross-linking, which ensures the dimensional stability of these promising biomaterials. Understanding swelling processes is essential, as they offer valuable insights into the diffusion capacity, fluid absorption, and dimensional stability of materials. Research on biopolymer-based interpenetrating gels offers significant potential for regenerative medicine, particularly in restoring the intervertebral nucleus pulposus.

Therefore, the primary aim of this study is to investigate how the preparation of a chitosan-based gel with different concentrations of PVA impacts not only the physical properties of the gel but also its potential to serve as an effective support for cell growth and tissue regeneration. Furthermore, by altering the concentrations of genipin, this study seeks to elucidate the impact of this variable on essential characteristics, including porosity, pore volume, interconnection density, fractal dimensions, and pore wall thickness. The preliminary results indicate that incorporating PVA as a dispersed and

interpenetrating phase markedly enhances the microarchitecture of the gel, surpassing that of gels composed solely of chitosan and genipin.

## Materials and Methods

### Preparation of Gel Formulations

The chitin used in this study was extracted from shrimp shells (*Litopenaeus vannamei*) at the B<sup>5</sup>IDA laboratory, and its derivative, chitosan (Ch), was obtained through a standard deacetylation reaction in an alkaline medium at elevated temperatures, resulting in a degree of deacetylation of 79%. This process followed the protocol outlined by Gallardo et al. (2019) [20]. The molecular weight of the Ch was determined using capillary viscometry, yielding a value of  $1.04 \times 10^5$  g/mol. The synthetic polyvinyl alcohol (PVA) (Himedia, USA) used in the study had a molecular weight of  $8 \times 10^4$  g/mol. The natural crosslinker, genipin (Gen), was extracted from the fruit of *Genipa americana*, purified in the B<sup>5</sup>IDA laboratory, and characterized following the protocol described by Colmenares et al. (2024) [12].

For the preparation of the interpenetrating network gels, stock solutions were prepared for each polymer, Ch and PVA. The Ch gel was prepared at a [2.5% w/v] concentration using a [1% v/v] acetic acid solution (Fluca Riedel-de Haen, 98%, Spain). The PVA solution was prepared at concentrations of [1% w/v] and [2% w/v] in deionized water. For the crosslinking agent, Gen crystals were dissolved in a 30% ethanol solution to obtain diluted solutions with concentrations of [0.010% w/v] and [0.025% w/v]. Each gel formulation was prepared by mixing equal volumes (1:1:1) of Ch/Gen/PVA, which were combined using a paddle mixer at 200 rpm for 10 minutes at room temperature. The interpenetrated gels formed were thoroughly washed by dialysis, and this procedure was repeated at least 2 times for each formulation before being taken to the lyophilization process (Labconco-Freezone 2.5, -45°C, and 1.5 Torr vacuum for 48 hours). The resulting xerogels, which are the focus of this study, were properly stored in desiccators, and the composition of each formulation is summarized in Table 1.

**Table 1** - Composition of each formulation of interpenetrated Ch/Gen/PVA gels.

Gel	F1 (% w/v)	F2 (% w/v)	F3 (% w/v)	F4 (% w/v)	F5 (% w/v)	F6 (% w/v)
Ch	2,5	2,5	2,5	2,5	2,5	2,5
Gen	0,010	0,025	0,010	0,025	0,010	0,025
PVA	0	0	1,0	1,0	2,0	2,0

### Morphological characterization of xerogels Microtomography (microCT)

The three-dimensional (3D) morphology of the scaffolds was investigated through microtomography (microCT) analysis. For this, a SkyScan1272 CMOS Edition microCT scanner (Bruker, Kontich, Belgium) was set up with these parameters: 20 kV source voltage, 100  $\mu$ A current, 4  $\mu$ m pixel size, 0.3° rotation steps from 0 to 180°, no filter, 4-frame averaging, and 2000 ms exposure time per image. The scanning time for each sample was approximately 2 hours.

NRecon software (v2.1.0.1, Bruker, Kontich, Belgium) was used to reconstruct X-ray projections, applying a 4% beam hardening correction, a 2-level ring artifact correction, and no smoothing. The 3D visualizations were generated using the CTvox software (v.3.3.1, Bruker, Kontich, Belgium) (Fig.1). To image analysis, the CTan software (version 1.20.8; 64-bit; Bruker microCT, Kontich, Belgium) was employed, in which the reconstructed images were subjected to binarization utilizing the Otsu 3D automatic segmentation algorithm [21,22]. Additionally, 3D noise removal operations, such as filtering and despeckle, were applied to improve image quality.

Subsequently, a comprehensive 3D morphometric analysis was conducted, which encompassed the evaluation of porosity (both closed and open), pore interconnectivity, degree of anisotropy, fractal dimension, as well as pore size distribution within the volume of interest.

### Scanning Electron Microscopy (SEM)

The morphological characteristics of the scaffold surfaces were analyzed using scanning electron microscopy (SEM) on a Tescan MIRA 3 (Korea). For each sample, a cryogenic cross-section was observed to examine the internal morphology of the xerogels and correlate these findings with the results obtained from microCT. Prior to observation, the samples were sputter-coated with gold to ensure adequate conductivity. During SEM imaging, a 15 kV accelerating voltage was applied in the Tescan microscope.

### Swelling Assay

Each xerogel sample, shaped as a cylindrical disk, was weighed and then immersed in a phosphate-buffered saline (PBS) solution at 37°C for a period of 36 hours, which is the time required

for all formulations to reach a constant weight and maintain physical stability. The immersion test was carried out in duplicate for each formulation, as well as the weighing was also carried out in duplicate, obtaining the error bars and represented in the result presented.

Based on the weight variation, the swelling ratio (Rh) was calculated using the following equation<sup>[12]</sup>:

$$Rh (\%) = [(W_{\text{hydrated}}(t) - W_{\text{xerogel}})] \times 100\% / (W_{\text{xerogel}}) \quad (\text{eq. 1})$$

where: W hydrated represents the weight of the hydrated xerogel as a function of time until equilibrium is reached; W xerogel corresponds to the weight of the dry xerogel (deshydrated gel). The experiment was conducted in triplicate using cylindrical samples to ensure accuracy and reproducibility of the results.

### Hemocompatibility

This assay was conducted in accordance with the ISO 10993-4 standard for biological evaluation of medical devices<sup>[23]</sup>. The hemolysis test was performed using blood agar, prepared according to the instructions provided by the manufacturer (Merck, Amsterdam). The agar base was cooled to 45 °C and mixed with sterile defibrinated sheep blood (INH Instituto Nacional de Higiene UCV, Caracas) to achieve a final concentration of 5% (v/v). The xerogel samples were sterilized by exposure to UV light for 15 minutes. Subsequently, the prepared blood agar was poured into sterile Petri dishes, and the xerogels were carefully placed onto the solidified agar. The Petri dishes were then incubated in a 5% CO<sub>2</sub>/95% air environment at 37°C for 48 hours. Finally, the results were documented photographically.

### Results and Discussion

It is well established that the pore architecture in hydrogels is a critical factor in determining their mechanical strength, fluid absorption capacity, and cell viability, while also significantly influencing cellular proliferation and differentiation<sup>[24-26]</sup>. Therefore, a thorough understanding of the pore morphology within a 3D structure is crucial, particularly when assessing its potential for biomedical, tissue engineering, and pharmacological applications. The results obtained from advanced techniques, such as SEM combined with microtomography (microCT), provide critical insights into this pore architecture and its degree of interconnectivity. Figure 1 shows representative images of the cross-sectional views of each xerogel, reconstructed using  $\mu$ CT and further examined transversally via SEM. As illustrated, the chitosan-based xerogels, regardless of the incorporation of genipin as a crosslinking agent or PVA as a dispersed and interpenetrating phase, exhibited a highly porous internal structure characterized by interconnected pores. This interconnected porosity is further confirmed by the

SEM micrographs accompanying the figure. The key microCT-derived parameters are summarized in Table 2.

Upon detailed examination, the morphology resulting from the blending of the natural polymer chitosan with the synthetic PVA showed no evidence of phase separation in any of the prepared formulations. This observation was confirmed through both SEM analysis and microtomography (microCT), which revealed consistent structural integrity across the entire network. Consequently, it can be considered that the hydrogels formed in this study exhibit the characteristics of a fully interpenetrated polymer network (IPN)<sup>[27]</sup>.

Moreover, when evaluating the effect of genipin concentration on the microstructure of each xerogel formulation, it was observed that lower concentrations of genipin resulted in a broader, more heterogeneous pore size distribution, whereas increasing the concentration of the crosslinking agent led to a narrower, more uniform distribution (Fig. 2). Specifically, at a genipin concentration of 0.010%, the pore sizes ranged from 180–340  $\mu$ m and 350–480  $\mu$ m, while at 0.025%, the distribution became more homogeneous, ranging from 220–340  $\mu$ m. This phenomenon can be attributed to the random nature of the crosslinking reaction: as the genipin concentration increases, the number of effective active crosslinking sites also increases, leading to greater uniformity. Additionally, the higher concentration of the interpenetrating PVA phase appears to further contribute to the improved uniformity in pore size distribution.

These results may be associated with the degree of anisotropy (DA), which appears to increase with higher genipin concentrations and the presence of the interpenetrating PVA phase. According to the literature, DA refers to the measurement of the preferential alignment of solid scaffolds in 3D structures along a particular direction<sup>[28]</sup>. In this context, the chitosan/PVA xerogels crosslinked with genipin demonstrated an almost two-fold increase in DA when the genipin concentration was raised. These values are consistent with porous scaffolds exhibiting porosities between 80–95%<sup>[22]</sup>. This suggests that genipin, as a crosslinking agent, may promote a more anisotropic properties in these scaffolds<sup>[29]</sup>.

According to the data presented in Table 2, the open pore volume and the total open pore percentage in the formulations ranged between 88–93%. However, a slight reduction in these percentages was observed as the genipin concentration increased. This result is consistent with the fact that higher genipin concentrations promote more extensive crosslinking reactions, leading to an increase in gel viscosity (hindering the mobility of molecular chains) and a higher crosslinking density, which generates a more stable 3D network.

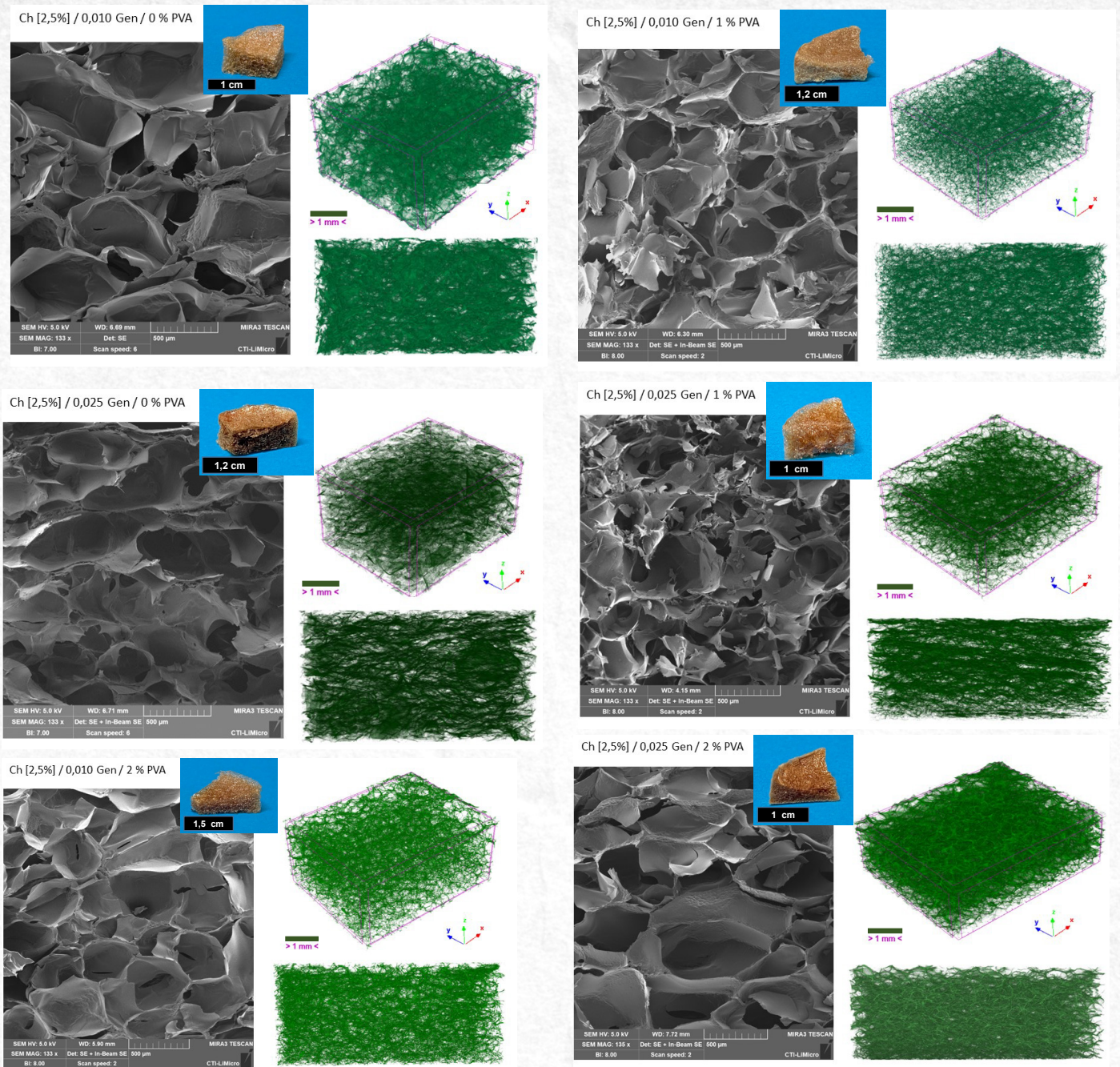


Figure 1 - View of each xerogel and their internal morphology as observed through SEM and X-ray microtomography techniques.

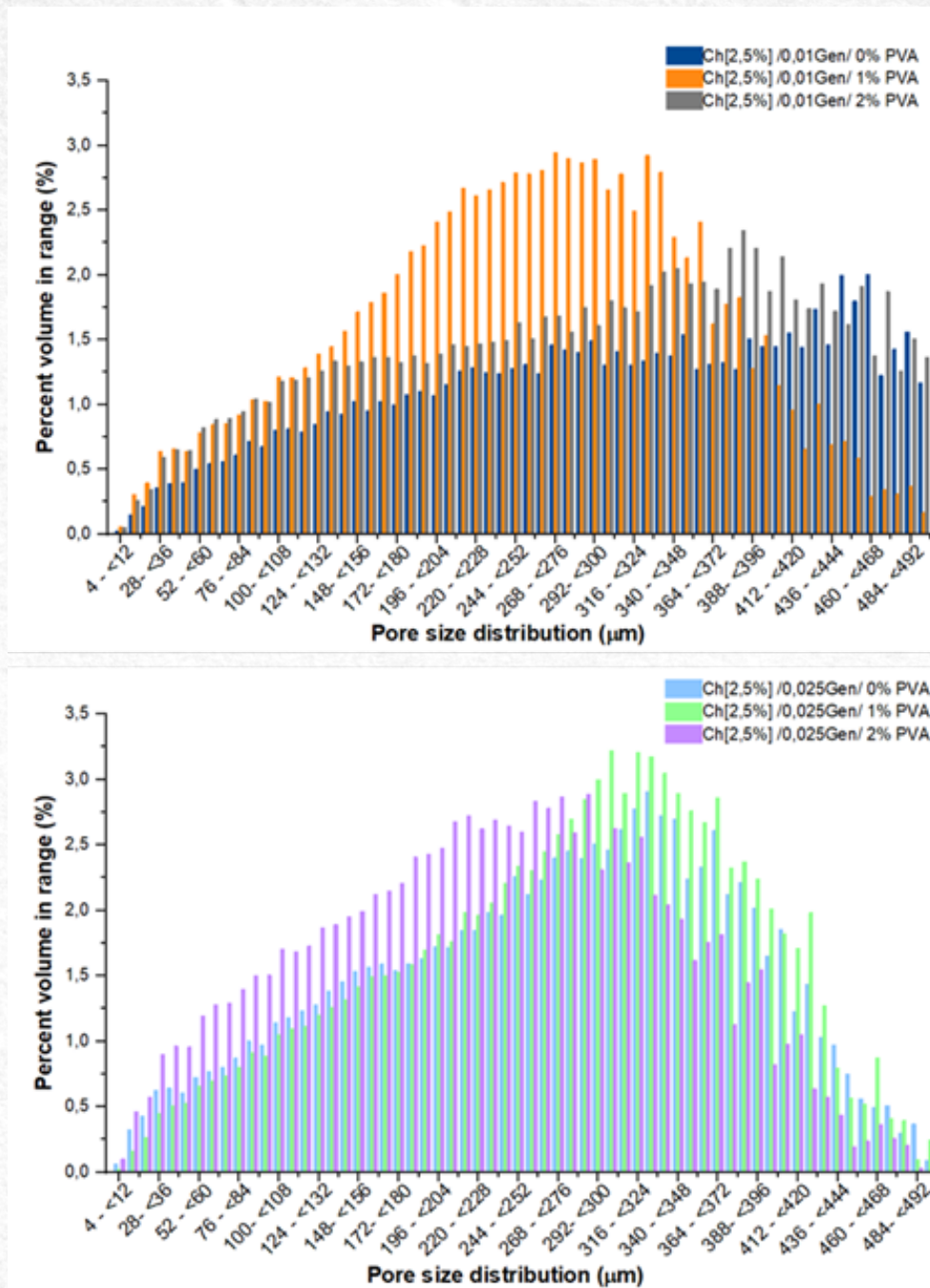


Figura 2 - Pore size distribution of each xerogel sample. Results obtained from microCT analysis.

**Table 2** - Morphometric Parameter Assessment. The data are represented for nearly 700-900 slices obtained after MicroCT imaging.

Parameter	Samples					
	F1	F2	F3	F4	F5	F6
Degree of Anisotropy (DA)	1,622	3,182	2,054	3,305	1,754	2,971
Volume of closed pores (mm <sup>3</sup> )	0,017	0,012	0,001	0,002	0,000	0,002
Closed porosity (%)	0,114	0,076	0,006	0,019	0,006	0,022
Volume of open pore space (mm <sup>3</sup> )	114,281	119,113	107,844	78,723	90,783	72,469
Open porosity (%)	88,743	88,086	92,621	90,911	92,971	89,295
Total volume of pore space (mm <sup>3</sup> )	114,298	119,126	107,844	78,725	90,784	72,471
Total porosity (%)	88,756	88,095	92,621	90,913	92,972	89,298
Connectivity	32360	73875	185848	132561	140807	122170
Fractal Dimension	2,472	2,542	2,533	2,464	2,467	2,576

This result is particularly promising, as studies in the field of tissue engineering scaffolds have reported that, in relation to the porous structure of biomaterials, smaller and more regular pore sizes improve the mechanical properties of the gel<sup>[30]</sup>. However, the pore size cannot be too small, otherwise it could have restrictions for the diffusion of biomolecules (such as certain proteins, nucleic acids, etc.). Furthermore, the diffusion of macromolecules that may be encapsulated and/or released from such structures is also enhanced<sup>[31]</sup>. Considering the use of these materials for cell culture studies, an adequate spatial distribution of cells deposited on the scaffold can be achieved, which facilitates a homogeneous distribution of the extracellular matrix. If the pores are too small, it may make it difficult for these essential elements to pass through, while if they are too large, they may not provide adequate support for cells. According to what the literature has reported, the pore size range is usually between approximately 75 to 500 micrometers<sup>[30-32]</sup>. This size allows cells to adhere and migrate through the scaffold, as well as facilitating the diffusion of nutrients and oxygen, as well as the removal of waste. And they should not be less than 20 microns. Consequently, this could initially promote cell proliferation and later differentiation<sup>[32]</sup>. Additionally, this ensures the vascularization processes characteristic of tissue regeneration<sup>[33]</sup>.

Additionally, increasing the proportion of PVA resulted in a decrease in pore size, although the pore size distribution became broader. The higher PVA content, acting as an interpenetrating and dispersed phase within the chitosan matrix, tends to elevate the viscosity of the mixture. This increased viscosity leads to a slower gelation rate, thereby promoting greater solvent evaporation, which indirectly raises the concentration of the solution over time. This

complex process results in the formation of more compact 3D structures, characterized by slightly smaller pores while preserving effective pore interconnectivity.

An important feature of all the xerogels obtained is their pore interconnectivity. The literature reports that such interconnectivity creates free volume, which facilitates cellular migration during the proliferation phase<sup>[34]</sup>, and thus supports the formation of the extracellular matrix and the movement of fluids, promoting vascularization throughout the molecular network<sup>[35]</sup>. Although no significant differences in this parameter were observed with increasing PVA content, the presence of the interpenetrated PVA phase did enhance pore interconnectivity compared to formulations with only the chitosan/genipin phase<sup>[36]</sup>.

Another critical parameter to evaluate is the fractal dimension (Df) of the hydrogels, a dimensionless index that characterizes the continuous and irregular geometry of three-dimensional networks and quantifies the complexity of their architecture<sup>[22, 37]</sup>. Previous studies have indicated that Df can significantly influence cellular behavior and is regarded as a key metric in the design and development of scaffolds for tissue engineering<sup>[22,28]</sup>. As shown in Table 2, our analysis revealed that the incorporation of genipin or PVA had no statistically significant effect on the Df of the xerogels, with values remaining similar across all cases, ranging from 2.4 to 2.6. These values can be attributed to the effective crosslinking of the chitosan and PVA polymer chains within the 3D network, despite compositional variations in the formulations. Furthermore, this crosslinking process did not negatively impact the total porosity, which remained at approximately 90%, nor did it compromise the

interconnectivity between pores, both of which are essential for maintaining the functionality of the scaffolds.

Regarding the thickness of pore walls (>80%) in the chitosan xerogels, no significant differences were found, regardless of the incorporation of genipin and PVA. Most pores exhibited a similar wall thickness, ranging from 12–20 μm to 28–36 μm, as shown in Fig. 3. However, when 1% PVA was used, the predominant wall thickness fell within the 12–20 μm range, whereas with 2% PVA, the predominant range expanded to 12–28 μm. This clearly confirms our hypothesis that genipin facilitates crosslinking

between chitosan chains, independent of the presence of an interpenetrated PVA phase, and that this helps improve pore connectivity (as previously demonstrated). This enhanced connectivity could improve fluid transport and enable the generation of three-dimensional structures with walls that ensure dimensional stability. This is an important consideration when developing structures with characteristics that could potentially biomimic those of an intervertebral disc component, specifically the nucleus pulposus, a central, gelatinous, yet mechanically resilient part [38].

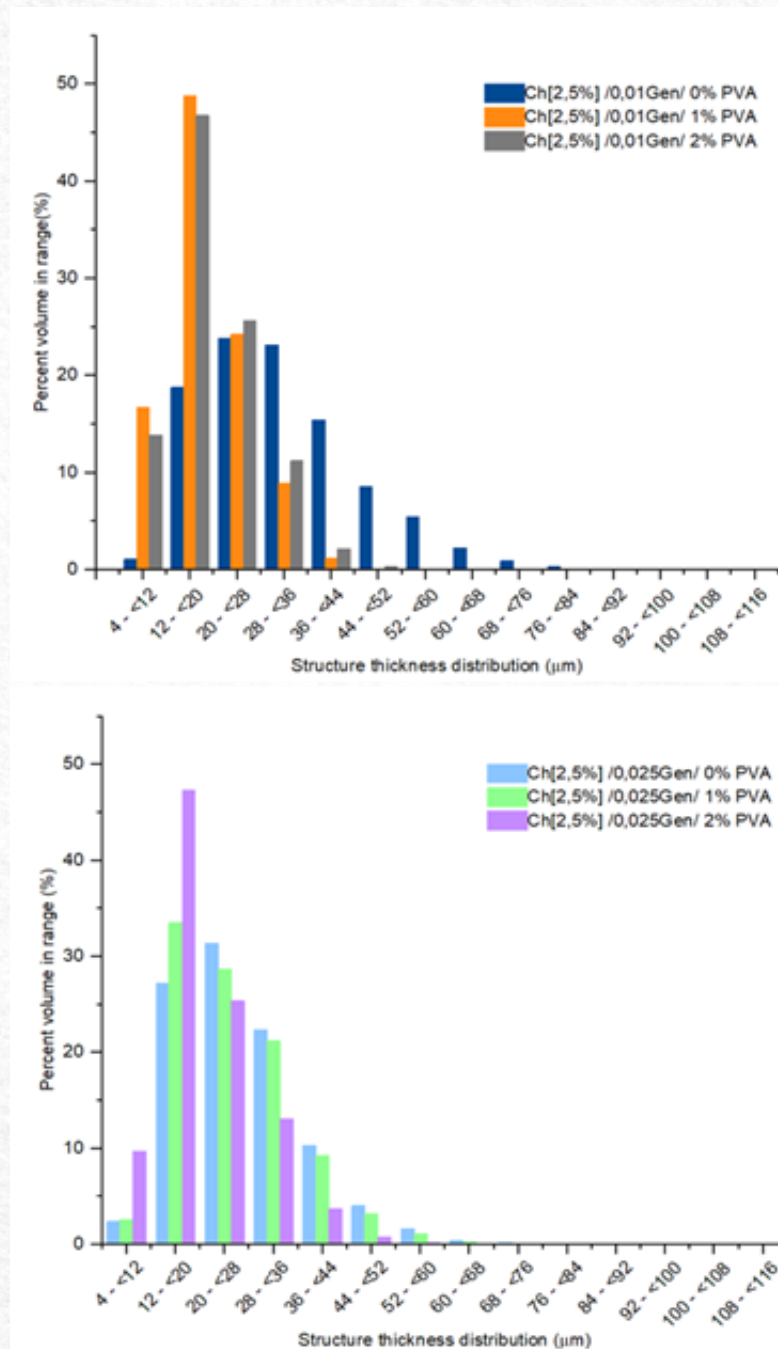


**Figure 3** - Effect of genipin and interpenetrated PVA phase in chitosan xerogels on pore wall thickness.

### Swelling Assay

At the macroscopic level, the swelling capacity of a hydrogel is determined by the amount of space within the polymer network that can be filled with fluid, the polymer-fluid interaction forces, electrostatic forces, and osmotic forces<sup>[39,40]</sup>. The first observation from the results shown in Fig. 4, is that all formulations behave as superabsorbent gels<sup>[40]</sup>, as in all cases the swelling ratio significantly exceeds 100%, with each sample maintaining its physical and dimensional stability when swollen. In most cases, thermodynamic equilibrium was reached after 28–30 hours, and no further water absorption (gravimetrically) or volume change was observed until the end of the experiment at 36 hours. This process, also known as Donnan equilibrium<sup>[41]</sup>, correlates the water absorption to the elimination of the osmotic pressure difference between the interior of the polymer network that forms the gel and the external solution in which the hydrogel is immersed<sup>[42,43]</sup>.

To explain this result, two fluid absorption mechanisms can be considered, both of which may describe the behavior observed in each formulation. The first mechanism is related to polymer-solvent

interactions, specifically the hydroxyl (-OH) groups interactions (from both PVA and chitosan), and the protonated amino groups (-[NH<sub>3</sub>]<sup>+</sup>) of chitosan with water molecules. The second mechanism involves the diffusion process through the free volume or space generated by the pores and their interconnectivity, which allows the solvent to permeate these areas, resulting in the relaxation of the Ch/PVA polymer chains that form the crosslinked network<sup>[44-46]</sup>.

According to the morphologies described in Figures 1–3 and the results summarized in Table 2, among the three components in each formulation, genipin not only acts as a crosslinking agent but also enhances the water absorption capacity, as evidenced by the increase in swelling percentage<sup>[40]</sup>. Additionally, the presence of PVA as an interpenetrated phase further supports this process, as these polymer chains not only improve pore interconnectivity but also contribute due to the hydrophilic nature of PVA and its greater elasticity compared to chitosan. This combination promotes better and greater molecular relaxation, allowing a significant amount of water to be retained within the gel without causing a loss of dimensional stability.

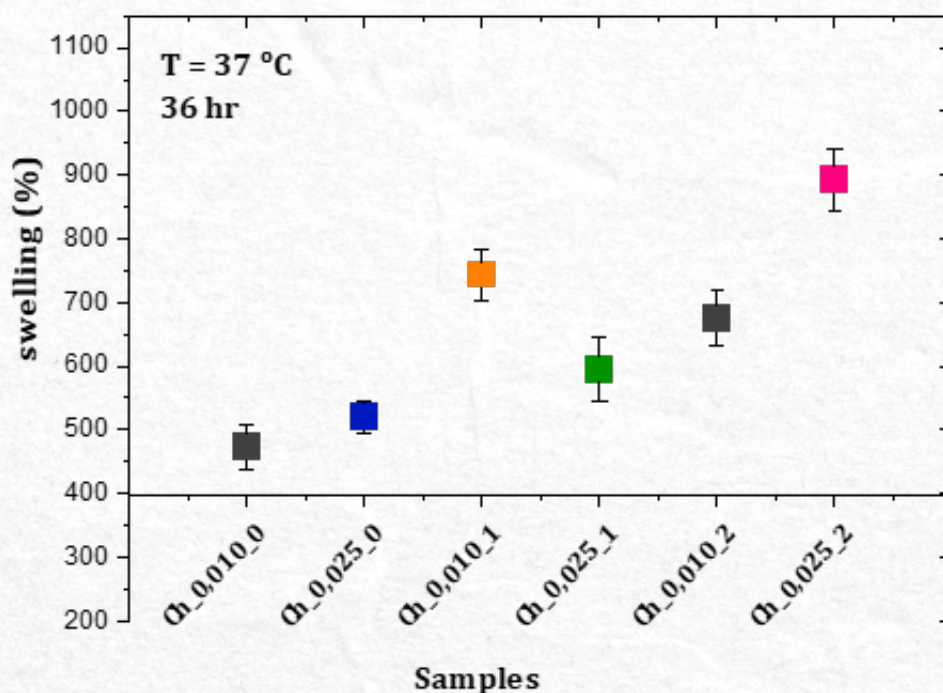


**Figure 4** – Swelling assay of xerogels under controlled time and temperature conditions. It is clear from the figure that the swelling behavior is influenced by the presence of the interpenetrated PVA phase in the chitosan matrix. Source: Own authorship, 2024

### Hemocompatibility

Among the essential requirements for a material to be used as an implant is biocompatibility, which is evaluated through a variety of experiments standardized by international technical norms (ISO 10993-4) [23]. One such test is the hemocompatibility assay. Hemolysis, or the lysis of blood cells, refers to the rupture of the cell membrane, allowing hemoglobin to be released from erythrocytes. There are three types of hemolysis: alpha, beta, and gamma. In alpha hemolysis, there is a partial breakdown of hemoglobin from erythrocytes. Beta hemolysis involves complete hemoglobin rupture, causing a "clearing" or whitening effect in the agar solution (known as a white halo). Gamma hemolysis, on the other hand, is not technically a hemolytic process but rather an oxidation process of the blood [9].

Figure 5 shows the evaluation of the xerogels in the blood-agar solution (as described in the experimental methodology). As can be seen, regardless of the genipin or PVA concentration within the studied range, no hemolysis was observed—neither alpha nor beta, and even the brown discoloration typical of gamma hemolysis was absent. As reported by Viera et al [9], where acrylamide was used as a positive control, showing a white halo due to hemotoxicity. This indicates that, under the experimental conditions tested, there was no hemolytic effect during the incubation period. In other words, these formulations did not cause the rupture of blood cell membranes, which is a positive indication of the potential of this biomaterial and opens a window for its application in tissue engineering. However, more complex cellular studies are still needed.

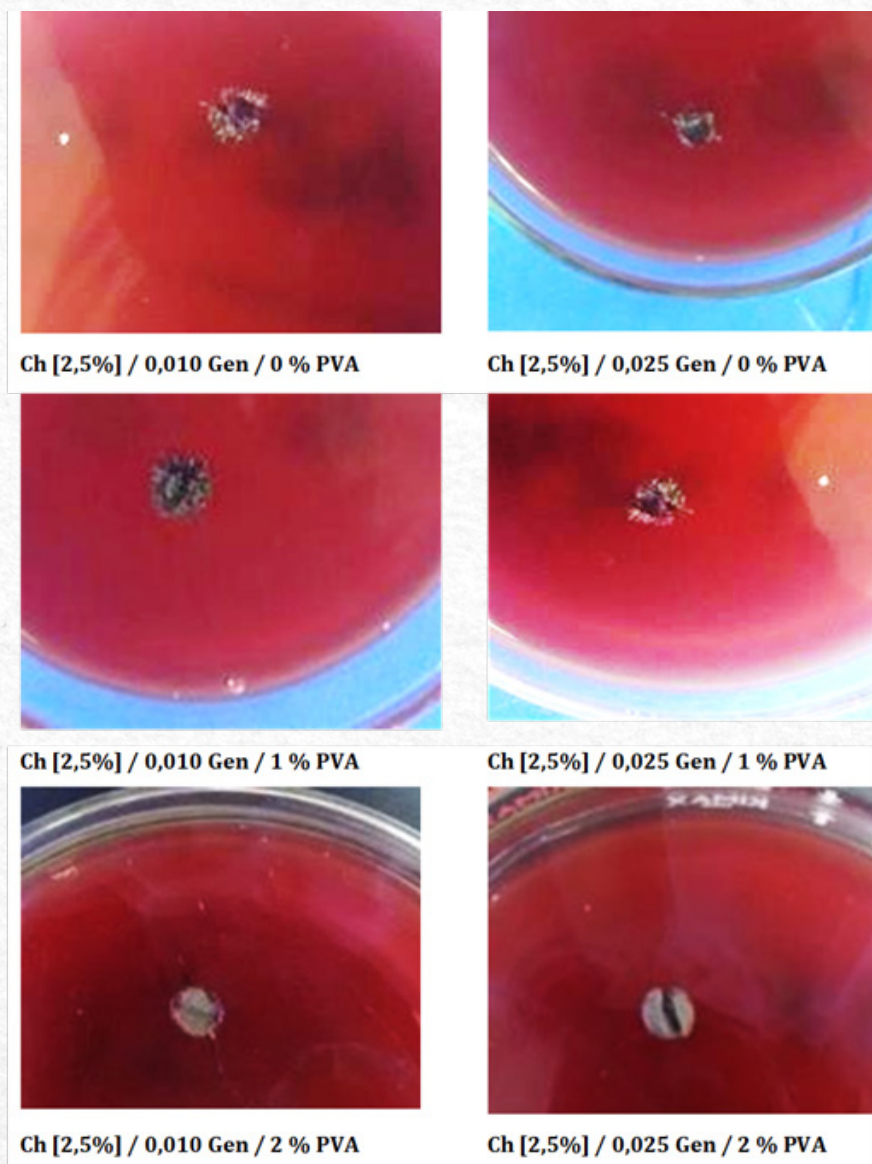


**Figure 5** - Agar-blood hemocompatibility assay for the evaluation of the studied xerogels, according to ISO 10993-4 standards. Source: Own authorship, 2024.

This result for the interpenetrated gels is not surprising, as numerous studies have reported that both chitosan (the primary polymer in the xerogels) and PVA (the dispersed phase) are non-toxic and do not elicit allergic or inflammatory responses via any route (implant, ingestion, or topical use)<sup>[47, 48]</sup>. Moreover, chitosan has been shown to exhibit antimicrobial, hypocholesterolemic, biodegradable, mucoadhesive and immunostimulant properties, among others<sup>[49]</sup>. Many studies have demonstrated its biocompatibility with various types of cells<sup>[49, 51]</sup>, and this cellular biocompatibility seems to increase with higher degrees of deacetylation. The chitosan used in this work had a degree of deacetylation of 79%. A higher degree of deacetylation means more free amino groups along the polysaccharide chain, which are responsible for promoting cell adhesion and proliferation<sup>[52]</sup>.

### Conclusions

The analysis of interpenetrated xerogels composed of chitosan, genipin, and PVA highlights the crucial influence of pore architecture and interconnectivity on their properties and potential applications. This was demonstrated through the use of innovative techniques, such as X-ray microtomography (microCT), complemented by scanning electron microscopy (SEM) results. It can be concluded that the incorporation of genipin serves as an effective crosslinker, allowing control over pore size distribution, while PVA, as an interpenetrating phase, enhances network interconnectivity, thereby providing a suitable environment for cell growth. These materials exhibit hemocompatibility and superabsorbent behavior. The ability to tune their structural properties further strengthens their potential as scaffolds for use in three-dimensional environments, positioning them as promising candidates for nucleus pulposus replacement in biomedical applications.

### Acknowledgment

The authors of this research dedicate it to the memory of Dr. Jorge Vicente Lopes da Silva, a pioneer of additive manufacturing in the Latin American region and the world. Their contribution during his life to our training and professional consolidation is shown in this research.

The authors also are grateful to the CNPq/PCI program (process nos. 301214/2024-7, 300038/2024-0 and 300933/2024-0) for the financial support.

### Declarations

### Conflict of Interest

All authors declare no conflict of interests.

### References

- [1]. Reddy MS, Ponnamma D, Choudhary R, Sadasivuni KK. A comparative review of natural and synthetic biopolymer composite scaffolds. *Polymers*. 2021 Mar 30; 13(7):1105. <https://doi.org/10.3390/polym13071105>
- [2]. Afewerki S, Sheikhi A, Kannan S, Ahadian S, Khademhosseini A. Gelatin-polysaccharide composite scaffolds for 3D cell culture and tissue engineering: towards natural therapeutics. *Bioeng Transl Med*. 2019 Jan; 4(1):96-115. <https://doi.org/10.1002/btm2.10124>
- [3]. Ma T, Liu C, Zhao Q, Zhang Y, Xiao L. Decellularized nucleus pulposus matrix/chitosan hybrid hydrogel combined with nucleus pulposus stem cells and GD-F5-loaded microspheres for intervertebral disc degeneration prevention. *Mol Med*. 2024 Jan 10; 30(1):7. <https://doi.org/10.1186/s10020-024-00777-z>
- [4]. Choi Y, Park MH, Lee K. Tissue engineering strategies for intervertebral disc treatment using functional polymers. *Polymers*. 2019 May 13; 11(5):872. <https://doi.org/10.3390/polym11050872>
- [5]. Santi S, Corridori I, Pugno NM, Motta A, Migliaresi C. Injectable scaffold-systems for the regeneration of spinal cord: advances of the past decade. *ACS Biomater Sci Eng*. 2021 Feb 1; 7(3):983-999. <https://doi.org/10.1021/acsbiomaterials.0c01779>
- [6]. Malaise S, Rami L, Montembault A, Alcouffe P, Burdin B, Bordenave L, Delmond S, David L. Bioresorption mechanisms of chitosan physical hydrogels: a scanning electron microscopy study. *Mater Sci Eng C*. 2014 Sep 1; 42:374-84. <https://doi.org/10.1016/j.msec.2014.04.060>
- [7]. Hildebrand T, Novak J, Nogueira LP, Boccaccini AR, Haugen HJ. Durability assessment of hydrogel mountings for contrast-enhanced micro-ct. *Micron*. 2023 Nov 1; 174:103533. <https://doi.org/10.1016/j.micron.2023.103533>
- [8]. Cui ZK, Kim S, Baljon JJ, Wu BM, Aghaloo T, Lee M. Microporous methacrylated glycol chitosan-montmorillonite nanocomposite hydrogel for bone tissue engineering. *Nat Commun*. 2019 Aug 6; 10(1):3523. <https://doi.org/10.1038/s41467-019-11511-3>
- [9]. Vieira JN, Posada JJ, Rezende RA, Sabino MA. Starch and chitosan oligosaccharides as interpenetrating phases in poly (N-isopropylacrylamide) injectable gels. *Mater Sci Eng C Mater Biol Appl*. 2014 Apr 1; 37:20-7. <https://doi.org/10.1016/j.msec.2013.12.005>
- [10]. Barbon S, Contran M, Stocco E, Todros S, Macchi V,

- Caro RD, Porzionato A. Enhanced biomechanical properties of polyvinyl alcohol-based hybrid scaffolds for cartilage tissue engineering. *Processes*. 2021 Apr 21; 9(5):730. <https://doi.org/10.3390/pr9050730>
- [11]. Romanczuk-Ruszk E, Sztorch B, Pakuła D, Gabriel E, Nowak K, Przekop RE. 3D printing ceramics—materials for direct extrusion process. *Ceramics*. 2023 Feb 1;6(1):364-85. <https://doi.org/10.3390/ceramics6010022>
- [12]. Colmenares LBH, Nejati M, Fang Y, Guo B, Jiménez-Quero A, Capezza AJ, Sabino MA. New sources of genipin-rich substances for crosslinking future manufactured bio-based materials. *RSC Sustain*. 2024;2(1):125-138. <https://doi.org/10.1039/D3SU00303E>
- [13]. Sabino MA, Garcia RA. Synthesis and characterization of S-IPN hydrogels of chitosan/PVA/PNIPAm to be used in the design of nucleus pulposus prosthesis. *Int J Adv Med Biotechnol*. 2020; 3(1):2-15. <https://doi.org/10.25061/ijamb.v3i1.30>
- [14]. ASTM International. Standard Practice for Assessment of Hemolytic Properties of Materials. ASTM F756-17. West Conshohocken, PA: ASTM International; 2017. 6p. <https://doi.org/10.1520/F0756-17>
- [15]. Nalezinková M. In vitro hemocompatibility testing of medical devices. *Thromb Res*. 2020 Nov; 195:146-150. <https://doi.org/10.1016/j.thromres.2020.07.027>
- [16]. Peñaranda JE, Sabino MA. Effect of the presence of lignin or peat in IPN hydrogels on the sorption of heavy metals. *Polym Bull*. 2010; 65:495-508. <https://doi.org/10.1007/s00289-010-0264-3>
- [17]. Ferreira KN, Girón JB, Gomes GH, Rodas AC, da Silva JV, Daguano JK, Sabino MA. Innovative thermosensitive alginate bioink combining cations for enhanced 3D extrusion bioprinting for tissue engineering. *Bioprinting*. 2024 Jun 1; 39: e00340. <https://doi.org/10.1016/j.bprint.2024.e00340>
- [18]. Mukasheva F, Moazzam M, Yernaimanova B, Shehzad A, Zhanbassynova A, Berillo D, Akilbekova D. Design and characterization of 3D printed pore gradient hydrogel scaffold for bone tissue engineering. *Bioprinting*. 2024 Jun 1; 39: e00341. <https://doi.org/10.1016/j.bprint.2024.e00341>
- [19]. Ziaie B, Velay X, Saleem W. Advanced porous hip implants: A comprehensive review. *Heliyon*. 2024 Sep 14;10(18): e37818. <https://doi.org/10.1016/j.heliyon.2024.e37818>
- [20]. Gallardo MGC, Barbosa RC, Fook MVL, Sabino MA. Síntesis y caracterización de un novedoso biomaterial a base de quitosano modificado con aminoácidos. *Matéria (Rio de Janeiro)*. 2019; 24. <https://doi.org/10.1590/S1517-707620190003.0710>
- [21]. Dixit K, Gupta P, Kamle S, Sinha N. Structural analysis of porous bioactive glass scaffolds using micro-computed tomographic images. *J Mater Sci*. 2020 Sep; 55:12705-24. <https://doi.org/10.1007/s10853-020-04850-w>
- [22]. Agarwal G, Agrawal AK, Fatima A, Srivastava A. X-ray tomography analysis reveals the influence of graphene on porous morphology of collagen cryogels. *Micron*. 2021 Nov 1; 150:103127. <https://doi.org/10.1016/j.micron.2021.103127>
- [23]. Nalezinková M. In vitro hemocompatibility testing of medical devices. *Thromb Res*. 2020 Nov 1; 195:146-50. <https://doi.org/10.1016/j.thromres.2020.07.027>
- [24]. Ran J, Xie L, Sun G, Hu J, Chen S, Jiang P, Shen X, Tong H. A facile method for the preparation of chitosan-based scaffolds with anisotropic pores for tissue engineering applications. *Carbohydr Polym*. 2016; 152:615-23. <https://doi.org/10.1016/j.carbpol.2016.07.054>
- [25]. Bi L, Cao Z, Hu Y, Song Y, Yu L, Yang B, Mu J, Huang Z, Han Y. Effects of different cross-linking conditions on the properties of genipin-cross-linked chitosan/collagen scaffolds for cartilage tissue engineering. *J Mater Sci Mater Med*. 2011; 22:51-62. <https://doi.org/10.1007/s10856-010-4177-3>
- [26]. Choi SW, Zhang Y, Xia Y. Three-dimensional scaffolds for tissue engineering: the importance of uniformity in pore size and structure. *Langmuir*. 2010; 26(24):19001-6. <https://doi.org/10.1021/la104206h>
- [27]. Banerjee S, Ray S, Maiti S, Sen KK, Bhattacharyya UK, Kaity S, Ghosh A. Interpenetrating Polymer Network (IPN): a novel biomaterial. *Int J Appl Pharm*. 2010; 2(1):28-33.
- [28]. Ghafar A, Parikka K, Haberthür D, Tenkanen M, Mikkonen KS, Suuronen JP. Synchrotron microtomography reveals the fine three-dimensional porosity of composite polysaccharide aerogels. *Materials*. 2017 Jul 28; 10(8):871. <https://doi.org/10.3390/ma10080871>
- [29]. Murab S, Gupta A, Włodarczyk-Biegun MK, Kumar A, van Rijn P, Whitlock P, Han SS, Agrawal G. Alginate based hydrogel inks for 3D bioprinting of engineered orthopedic tissues. *Carbohydrate Polymers*. 2022 Nov 15; 296:119964. <https://doi.org/10.1016/j.carbpol.2022.119964>

- [30]. Jamali SA, Mohammadi M, Saeed M, Haramshahi SM, Shahmahmoudi Z, Pezeshki-Modaress M. Biomimetic fiber/hydrogel composite scaffolds based on chitosan hydrogel and surface modified PCL chopped-microfibers. *Int J Biol Macromol.* 2024 Oct 1; 278:134936. <https://doi.org/10.1016/j.ijbiomac.2024.134936>
- [31]. Liu B, Chen K. *Advances in Hydrogel-Based Drug Delivery Systems.* *Gels.* 2024 Apr 13; 10(4):262. <https://doi.org/10.3390/gels10040262>
- [32]. Yin S, Wu H, Huang Y, Lu C, Cui J, Li Y, Xue B, Wu J, Jiang C, Gu X, Wang W. Structurally and mechanically tuned macroporous hydrogels for scalable mesenchymal stem cell-extracellular matrix spheroid production. *Proc Natl Acad Sci U S A.* 2024 Jul 9; 121(28). <https://doi.org/10.1073/pnas.2404210121>
- [33]. Zeltinger J, Sherwood JK, Graham DA, Mueller R, Griffith LG. Effect of pore size and void fraction on cellular adhesion, proliferation, and matrix deposition. *Tissue Eng.* 2001; 7(5):557-72. <https://doi.org/10.1089/107632701753213183>
- [34]. Wu X, Huo Y, Ci Z, Wang Y, Xu W, Bai B, Hao J, Hu G, Yu M, Ren W, Zhang Y. Biomimetic porous hydrogel scaffolds enabled vascular ingrowth and osteogenic differentiation for vascularized tissue-engineered bone regeneration. *Appl Mater Today.* 2022 Jun 1; 27:101478. <https://doi.org/10.1016/j.apmt.2022.101478>
- [35]. Xu Z, Li J, Zhou H, Jiang X, Yang C, Wang F, Pan Y, Li N, Li X, Shi L, Shi X. Morphological and swelling behavior of cellulose nanofiber (CNF)/poly (vinyl alcohol) (PVA) hydrogels: poly(ethylene glycol) (PEG) as porogen. *RSC Adv.* 2016; 6:43626-33. <https://doi.org/10.1039/C6RA03620A>
- [36]. Olăreț E, Stancu IC, Iovu H, Serafim A. Computed tomography as a characterization tool for engineered scaffolds with biomedical applications. *Materials.* 2021 Nov 10; 14(22):6763. <https://doi.org/10.3390/ma14226763>
- [37]. Zoetebier B, Schmitz TC, Ito K, Karperien M, Tryfonidou MA, Paez JI. Injectable hydrogels for articular cartilage and nucleus pulposus repair: status quo and prospects. *Tissue Eng Part A.* 2022 Jun 1; 28(11-12):478-99. <https://doi.org/10.1089/ten.tea.2021.0226>
- [38]. Sabino MA, Garcia RA. Synthesis and characterization of S-IPN hydrogels of chitosan/PVA/PNIPAm to be used in the design of nucleus pulposus prosthesis. *Int J Adv Med Biotechnol.* 2020; 3(1):2-15. <https://doi.org/10.25061/ijamb.v3i1.30>
- [39]. Wang T, Turhan M, Gunasekaran S. Selected properties of pH-sensitive, biodegradable chitosan-poly(vinyl alcohol) hydrogel. *Polym Int.* 2004; 53:911-8. <https://doi.org/10.1002/pi.1461>
- [40]. Baker JP, Stephens DR, Blanch HW, Prausnitz JM. Swelling equilibria for acrylamide-based polyampholyte hydrogels. *Macromolecules.* 1992 Mar; 25(7):1955-8. <https://doi.org/10.1021/ma00033a019>
- [41]. Boyd LM, Carter AJ. Injectable biomaterials and vertebral endplate treatment for repair and regeneration of the intervertebral disc. *Eur Spine J.* 2006 Aug; 15 Suppl 3. <https://doi.org/10.1007/s00586-006-0172-2>
- [42]. Longmi F, Tan YC, Liang HC. In vitro evaluation of a chitosan membrane cross-linked with genipin. *J Biomater Sci Polym Ed.* 2001; 12(8):835-50. <https://doi.org/10.1163/156856201753113051>
- [43]. J. Anderson JM. Biological responses to materials. *Annu Rev Mater Res.* 2001; 31:81-110. <https://doi.org/10.1146/annurev.matsci.31.1.81>
- [44]. Zhang JT, Cheng SX, Zhuo RX. Poly (vinyl alcohol)/poly (N-isopropylacrylamide) semi-interpenetrating polymer network hydrogels with rapid response to temperature changes. *Colloid Polym Sci.* 2003; 281:580-3. <https://doi.org/10.1007/s00396-002-0829-2>
- [45]. Chau M, De France KJ, Kopera B, Machado VR, Rosenfeldt S, Reyes L, et al. Composite hydrogels with tunable anisotropic morphologies and mechanical properties. *ACS Appl Mater Interfaces.* 2016; 28(10):3406-15. <https://doi.org/10.1021/acs.chemmater.6b00792>
- [46]. Wang B, Wu X, Li J, Hao X, Lin J, Cheng D, Lu Y. Thermosensitive behavior and antibacterial activity of cotton fabric modified with a chitosan-poly (N-isopropylacrylamide) interpenetrating polymer network hydrogel. *Polymers.* 2016; 8:1-11. <https://doi.org/10.3390/polym8040110>
- [47]. Desai LS, Lister L. Biocompatibility safety assessment of medical devices: FDA/ISO and Japanese guidelines. *Toxikon Corp.* 2016; 1-19.
- [48]. Sun K, Li ZH. Preparations, properties and applications of chitosan based nanofibers fabricated by electrospinning. *Express Polym Lett.* 2011 Apr 1; 5(4):342- 61 <https://doi.org/10.3144/expresspolymlett.2011.34>
- [49]. Mohebbi S, Nezhad MN, Zarrintaj P, Jafari SH, Gholizadeh SS, Saeb MR, Mozafari M. Chitosan in biomedical engineering: a critical review. *Curr Stem Cell Res Ther.* 2019 Feb 1; 14(2):93-116. <https://doi.org/10.2174/1574888X13666180912142028>

- [50]. Qi Y, Jiang X, Meng Z, Wu X. Modified chitosan thermosensitive hydrogel enables sustained and efficient anti-tumor therapy via intratumoral injection. *Carbohydr Polym.* 2016; 144:245-53. <https://doi.org/10.1016/j.carbpol.2016.02.059>
- [51]. Baxter A, Dillon M, Taylor KDA. Improved method for I.R. determination of the degree of N-acetylation of chitosan. *Int J Biol Macromol.* 1992; 14:166-9. [https://doi.org/10.1016/S0141-8130\(05\)80007-8](https://doi.org/10.1016/S0141-8130(05)80007-8)
- [52]. Chiellini F, Ottenbrite RM, Chiellini E, Dash M. Chitosan: a versatile semi-synthetic polymer in biomedical applications. *Prog Polym Sci.* 2011; 36:981-1014. <http://dx.doi.org/10.1016/j.progpolymsci.2011.02.001>